Investigating the effect of biofouling on propeller characteristics using CFD

David Owen, Yigit Kemal Demirel*, **Elif Oguz, Tahsin Tezdogan and Atilla Incecik**

Department of Naval Architecture, Ocean and Marine Engineering, University of Strathclyde,
100 Montrose Street, Glasgow, G4 0LZ, UK

**corresponding author;* e-mail: yigit.demirel@strath.ac.uk, phone: +44(0)1415483463

ABSTRACT

Increasing pressure is being placed on the marine industry to address ship emissions, regulations to govern the efficient operation of ships in the form of the Energy Efficiency Design Index (EEDI) and Energy Efficiency Operation Index (EEOI) have recently come into force. All aspects of ship design and operation that impact the energy efficiency of ships are subject to revaluation. This paper investigates the detrimental effects of biofouling on the performance of Potsdam Propeller Test Case (PPTC) propeller using Computational Fluid Dynamics (CFD). A previously-developed CFD approach for approximating the surface roughness due to biofouling has been applied in order to predict the effects on propeller characteristics. The roughness effects of a typical coating and different fouling conditions on the propeller performance were predicted for various advance coefficients. The effect proved to be drastic with the most severe fouling condition resulting in a 11.94% efficiency loss at J=0.6 ranging to an alarming 30.33% loss at J=1.2 compared to the smooth condition. The study acts as a proof of concept for the proposed CFD assessment method which can be used as a very practical approach to predicting the impact of realistic fouling conditions on propeller characteristics and energy efficiency.

Keywords: Biofouling, CFD, Propeller, Open Water

1. INTRODUCTION

Shipping is the most efficient mode of transport when compared against land and aviation counterparts. The rising world population and globalisation have resulted in increased shipping traffic and this trend will continue as shipping is the only effective means of transporting the world's cargo. This will cause greater greenhouse gas (GHG) emissions in the sector.

The recent introduction of regulatory legislation for ship emissions in the maritime industry has brought about the need for improving energy efficiency for environmental benefits. Although ships have been identified to be one of the most efficient modes of bulk transportation in terms of emissions per tonne of cargo carried, a study carried out by the International Maritime Organisation (IMO, 2009) indicated that potential energy efficiency improvements could be attained using both technological and operational methods. IMO's GHG study in 2007 reported that shipping emitted around 1046 tonnes of greenhouse gases for that same year. This amounts to 3.3% of global emissions with 870 tonnes arising from CO_2 making this the most prevalent gas emitted by ships. This is closely followed by SOx and NOx, which are addressed separately within the industry, however reducing the amount of fuel consumed by a vessel will naturally also have a positive impact on the emission of these gases. A projection outlined by Fang et al. (2013) indicated a significant increase of the world seaborne trade in the near future, predicting it to double by 2030. The increase in shipping volume will lead to an increase in ship emissions and IMO's second GHG study indicated that in the absence of strict policies, by the year 2050, ship emissions could multiply by a factor of around 2 to 3 times that of current levels. This therefore identifies a problematic issue, one that requires attention and recognition as concern grows and the need for improving energy efficiency to minimise emissions from the shipping sector becomes more important.

An Energy Efficiency Design Index (EEDI) (IMO, 2014) was therefore developed by a specialist group of the IMO known as the Marine Environmental Protection Committee (MEPC) as an incentive to control and lower Green House Gas emissions. The Designed EEDI of a vessel is estimated by calculating the predicted carbon emissions emitted compared to the useful work done by the ship (i.e. tonnes of cargo transported per nautical mile). EEDI restriction values assigned by the IMO differ by ship type and size. EEDI regulations were enforced on the 1st January 2013 and a phased implementation plan will see the restrictions become more stringent, currently the most demanding phase intended for implementation is in 2025.

Nomenclature				
k_s	equivalent sand grain roughness height		n	revolutions
Rt_{50}	average hull roughness		V_a	advance velocity
ΔU^+	roughness function		J	non-dimensional advance coefficient
k^+	roughness Reynolds number		η	propulsion efficiency
κ	von Karman constant		$P_{0.7}/D$	pitch ratio r/R=0.7
y^+	non-dimensional wall distance		A_E/A_O	area ratio
ρ	density		$C_{0.7}$	chord length$_{0.7}$
$\overline{u}_i$	averaged Cartesian components of the velocity vector		θ	skew (deg)
$\rho\overline{u_i'u_j'}$	Reynolds stresses		D_h/D	hub Ratio
p	mean pressure		Z	number of blades
$\overline{\tau}_{ij}$	mean viscous stress tensor components		p_a	apparent order
μ	dynamic viscosity		r, r_{21}, r_{32}	grid refinement factors
T	thrust		ϕ_k	key variable on the k^{th} grid
Q	torque		ϕ_{ext}^{21}	extrapolated value
K_T	thrust coefficient		e_a^{21}	approximate relative error
K_Q	torque coefficient		e_{ext}^{21}	extrapolated relative error
D	propeller diameter		GCI_{fine}^{21}	fine-grid convergence index

The regulations in their current form are acknowledged to have some shortcomings, however any changes are unlikely to substantially change the overall aim of these regulations.

Ambitions to improve energy efficiency in vessel operations are commonly shared with ship owners seeking to cut down fuel costs and expenses. The total ship transportation cost breakdown has changed significantly in recent years. Prior to 2008, the initial capital expenditure of a vessel was the main cost when compared to the operational and bunker cost throughout a ship's lifetime. With operating costs maintaining a constant rate throughout the years and bunker prices becoming volatile where sudden spikes in price are common, the fuel costs of a vessel are becoming more significant. Hence, with the continuing volatility of fuel costs, a vessel's fuel consumption has become a ship owner's prime concern which leads directly to considering the energy efficiency of the vessel (Hansen et al., 2011).

There are many ways to decrease the amount of fuel used, for example by autopilot upgrades and waste heat recovery systems. Such systems have high installation costs whilst savings are difficult to calculate. Another option of reducing speed is not practical for all vessel types.

The International Council on Clean Transport (ICCT) researched potential methods to achieve the required reductions, considering the propeller as a key area of potential improvement (ICCT, 2011). A propeller upgrade is one method but since much research is conducted before the initial selection, this only tends to occur when the propeller is damaged and must be replaced. Propeller polishing is another option, this study revealed that it exhibits a greater CO_2 reduction potential (~5% with a maximum of 8%) than both propeller upgrade and weather routing as shown in Figure 1. This magnitude is also close to that of cleaning the hull which is an uncommon realisation.

It has also been shown that the cost to achieve this reduction is one of the lowest, making it both cheap and effective. A study by Hydrex Underwater Technology projected potential fuel savings of 5% (Hydrex, 2017). This establishes that preventing biofouling accumulation on the propeller could play an important role in reaching EEDI/EEOI targets for ship operators.

Hull cleaning and propeller polishing are both used to remove any undesired fouling particles that have attached on the surface. The effect of fouling on a propeller is not given as much attention as hull fouling and hence there is a lack of material on this subject. One possible reason is that it is difficult to study using model-scale experiments due to possible scaling issues and the need to recreate many different sample types representing all relevant fouling particles. Korkut and Atlar (2012) experimentally investigated the effect of foul release coatings on the hydrodynamic performances of propellers and demonstrated the difficulties of model-scale experiments.

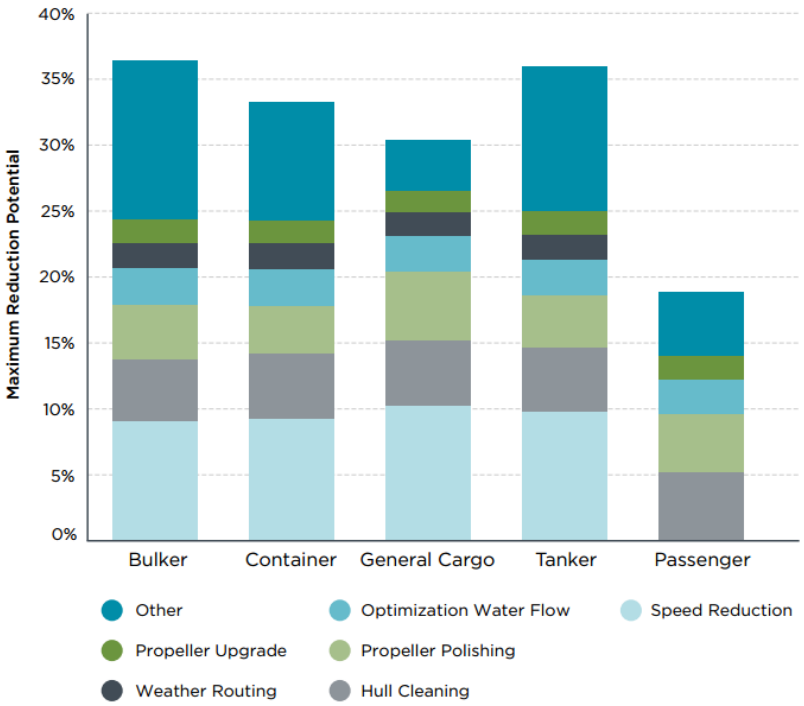

Figure 1: CO_2 reductions of technical and operational measures by ship types (ICCT, 2011)

Ship energy consumption depends on the performance of different components of the ship system; one significant component being the ships' hydrodynamic system comprising of the hull resistance, propulsion efficiency and hull-propeller interaction. These aspects can be addressed in a number of ways, both in terms of design and operation. For instance, some studies ((Kawamura et al., 2012), (Hansen et al., 2011), (Patience and Atlar, 1998), (Schuiling, 2013)) suggest that the installation of Energy Saving Devices (ESDs) on a ship can result in a significant improvement in energy efficiency. From an operational perspective, marine biofouling is an increasing problem from both economic and environmental points of view in terms of increased resistance, increased fuel consumption, increased GHG emissions and transportation of harmful non-indigenous species (NIS). It should be noted that even a small amount of fouling may lead to a non-negligible increase in fuel consumption. Due to its negative effects on ship efficiency and the marine environment, it is very desirable to mitigate the accumulation of biofouling on ship hulls. While improving the energy efficiency of existing ships by applying new antifouling paints, it is equally important to accurately model and understand the potential effects of biofouling on ship resistance and propeller characteristics and to demonstrate the importance of the mitigation of such effects by carrying out scientific research. The (ITTC, 2011a) therefore recommends researchers to develop new formulae or methods, using experimental data for validation, for the prediction of the effects of coatings and biofouling on ship performance. With the increased availability of computational power

and advances in numerical tools and modelling software, the use of numerical procedures are becoming more popular in aiding to maximise the energy efficiency saving potential.

There is therefore the need for a practical and realistic approach to predicting this impact of fouling on ship energy efficiency, which is accessible for designers, and can be applied within realistic timescales and without significant expense. In this context CFD approaches have the advantage over experimental approaches, since the use of CFD may eliminate the significant expense of a large amount of models and test runs that would be required.

To the best of the authors' knowledge, no specific CFD model exists at present to predict the roughness effect of biofouling on propeller performance. The aim of the present paper is therefore to fill this gap by employing the CFD model proposed by Demirel (2015) and Demirel et al. (2017a) for propeller analysis. This study may therefore be considered as an extension of the study presented in Demirel (2015) and Demirel et al. (2017a). The proposed CFD approach enables the prediction of the propeller characteristics of model-scale 3D propellers bearing a typical coating and a range of fouling conditions.

The authors believe that the question of how to correlate the roughness functions of fouled surfaces with the measurable parameters is a question far from being answered and a single measurable parameter is not enough to represent the surface roughness characteristics. For this reason, rather than trying to correlate measurable surface properties with this roughness function model, for each test surface equivalent sand roughness height, k_s can be obtained using reverse engineering (Demirel et al., 2017b). This is the height of uniform, closely-packed sand which gives the same roughness function as the roughness of interest in the fully rough flow regime (Schultz, 2007). It should be noted that equivalent sand roughness heights are not a function of measurable surface properties and they are experimentally obtained for each surface. The main advantage of the proposed CFD model is that it enables the use of a simple roughness length scale, k_s, to predict the effect of biofouling on the performance characteristics of a propeller, similar to that of Demirel et al. (2014, 2017a).

The initial step of the investigation was to validate the open water numerical simulation approach by comparing results with experimental values at model scale for a well-known benchmarking case, the Potsdam Propeller Test Case (PPTC). The numerical model was then modified to account for biofouling effects of different degrees in order to analyse the impact on propeller characteristics. The results then present the impact that different levels of fouling have on the thrust and torque coefficients and hence the open water efficiency of the propeller, at various different advance coefficients.

2. BACKGROUND

2.1 Literature Review

This section gives an overview of the work conducted on the topic of biofouling on marine propellers using CFD. It should be noted that as this is a very specific area, there are not a plethora of sources on this topic, but on the other hand research has been conducted in similar areas such as the impact of anti-fouling (AF) coatings on the propeller, the impact of fouling on the ship hull and optimisation of propeller design using CFD. These studies give a valuable insight into the work conducted in the field, but ultimately conclude that at present research has been conducted into propeller design and to a smaller degree fouling, but there is insufficient research on the impact of these studies combined.

Schultz, 2007 demonstrated that fouling on the hull could cause as high as an 86% powering penalty with heavy calcareous fouling. Similarly, Demirel et al. (2017a) predicted the increase in effective power required for a container vessel with heavy calcareous fouling travelling at 24 knots to be 108%. A recent study of Demirel et al. (2017b) demonstrated that even 10% coverage of barnacles each 5mm in height can increase the effective power of a container vessel by up to 46%. These studies prove that the presence of fouling on the hull will cause significant losses.

Townsin et al. (1981) recognised that propeller fouling "can be as destructive of fuel economy as rough hulls but the remedy is much cheaper". He used sand grain roughness to predict the increased drag. Mosaad (1986) recognised that although propeller losses may seem less severe than through the hull form, the losses per unit area are much greater. An analytical method was proposed to calculate the effect on ship performance of a rough hull and propeller combined with some thorough case studies. Atlar et al. (2003a) used a Rubert propeller roughness comparator followed by estimations of increased drag on blade sections and computer software to determine the efficiency lost due to fouling on a merchant ship. A propeller one-two years into service with no coating is represented by Rubert surface roughness F (252μm) and compared to a coated propeller the efficiency loss can be as high as 6%. This occurs through the increased torque and reduced thrust produced by the rougher propeller surface. Extending this study to high speed vessels Atlar et al. (2003b) found that for the normal design condition the loss in efficiency due to a Rubert F surface roughness for this vessel to be 11%, almost double that seen for the merchant ship. From this they identified that there was an increased efficiency saving potential for high speed craft such as military vessels if the accumulation of

fouling could be prevented. Analysing the work of Atlar et al. (2003b), Anderson et al. (2003) recognised that cleaning the propeller offers a "high return from a relatively low investment" with additional benefits of reduced cavitation and noise.

Seo et al. (2016) estimated a 9.5% loss in propeller efficiency with heavy slime condition and 14.6% due to small calcareous fouling, concluding that a clean propeller is vitally important in determining propulsion efficiency.

In a recent study, it was found that if an antifouling coating was applied correctly to the propeller, it would be possible to avoid performance decreases due the coating itself whilst benefiting from a decreased ability for marine organisms to attach (Korkut and Atlar, 2012).

Conversely, such coatings are rarely applied to the propeller due to assumptions that the copper/bronze surface already acts as an anti-fouling system which is not always the case. Furthermore, some coatings are toxic and can leach out to the environment after some deterioration occurs, whilst others are less toxic but also more expensive and less effective.

Many of the experiments investigating surface roughness model simple geometries such as flat plates or a barge shaped vessel whereas propeller geometry is comparatively complex. In addition, due to the variation of biofouling organisms and the severity of the accumulation, a high number of samples would be required to build an understanding of its effect.

Granville (1958, 1978) proposed a similarity law scaling procedure for the prediction of the effects of a particular surface roughness on the frictional resistance of any arbitrary body covered with the same roughness, utilising experimentally obtained quantities. Grigson (1985) proposed a method which is partly experimental and partly theoretical, just like the ones proposed by Granville. When it comes to CFD-based models, there are fewer studies investigating the roughness effects of coatings and biofouling on ship resistance. Currently, physical modelling of the roughness sources, such as coatings or biofouling in CFD is practically impossible due to their complex geometries. However, once the relationship of $\Delta U^+ = f(k^+)$ is known, where ΔU^+ is the roughness function and k^+ is the roughness Reynolds number, it can be employed in the wall-function of the turbulence models of the CFD software, as discussed by Patel (1998). The use of CFD-based unsteady RANS models is of vital importance, since the phenomenon can be simulated by means of a fully non-linear method. High power computer facilities are now more readily available than towing tanks allowing a more in-depth study to be performed in a shorter time frame. Having said that, while CFD provides accurate results when used properly, experimental data is still a necessity for the validation of CFD models and the development of accurate CFD prediction methods.

Several studies exist which model the effects of a uniform sand-grain roughness either using wall-functions (e.g. (Suga et al., 2006), (Apsley, 2007)) or using near-wall resolution (e.g. (Krogstad, 1991), (Aupoix, 2007)). Eça and Hoekstra (2011) showed that the effect of uniform sand-grain roughness on the frictional resistance of flat plates of full-scale ship lengths at full-scale ship speeds could be accurately simulated using either wall-functions or near-wall resolution. Khor and Xiao (2011) investigated the effects of fouling and two antifouling coatings on the drag of a foil and a submarine by employing a CFD method. They used the equivalent sand grain roughness height and the built-in wall-function which considers the uniform sand-grain roughness function model proposed by Cebeci and Bradshaw (1977), based on Nikuradse's data (Nikuradse, 1933). Castro et al. (2011) carried out unsteady RANS CFD simulations of a full-scale KCS model with hull roughness using wall-functions. However, they used a constant roughness function and roughness allowance formulation proposed by the ITTC (1990). Recently, Haase et al. (2016) applied CFD approach to predict the sand grain roughness effects on the frictional resistance of flat plates as well as on the resistance of catamarans. However, the ITTC (2011b, 2014) agreed the sand grain roughness function does not give accurate representation of surface roughness or fouling and encouraged new methods to be developed. It is known that the built-in roughness function model is based on uniform, closely packed sand roughness in CFD applications while the roughness function of real engineering surfaces do not show this behaviour.

2.2 Propulsion Characteristics

In order to characterise the design performance of a propeller its open water and after-hull properties should be described. The first term expresses the behaviour of the propeller in uniform flow with a steady load while the second term illustrates moment and forces for a propeller in a mixed wake field experiencing steady and unsteady loads. Generally, propeller designs are compared by analysing their thrust (T) and torque (Q) in an open water environment. Most importance is placed on the force produced by the propeller, thrust (T) and the moment produced, torque (Q). To allow adequate comparison, these are expressed as non-dimensional coefficients, namely thrust coefficient (K_T) and torque coefficient (K_Q), using standard relations as in Equations 1 and 2.

$$K_T = \frac{T}{\rho n^2 D^4} \tag{1}$$

$$K_Q = \frac{Q}{\rho n^2 D^5} \tag{2}$$

where D is the propeller diameter, ρ is the water density, and n denotes the revolutions per second. K_Q is often expressed as 10 K_Q since this normally results in a value of the same order as K_T. The advance velocity is defined as V_a, thus a non-dimensional advance coefficient, J, is shown in Equation 3.

$$J = \frac{V_a}{nD} \tag{3}$$

Thrust (K_T) and torque (K_Q) coefficients can be used to evaluate the propulsion efficiency (η) (Equation 4).

$$\eta = \frac{K_T}{K_Q} \times \frac{J}{2\pi} \tag{4}$$

To identify the optimum efficiency and operating point of a propeller, thrust and torque coefficients should be plotted for a range of advance coefficients (J) producing propeller curves.

3. NUMERICAL MODELLING

3.1. Mathematical formulation

A Reynolds-Averaged Navier-Stokes (RANS) method was used to solve the governing equations in this study. These mass and momentum conservation equations were solved by the commercial CFD software STAR-CCM+. The averaged continuity and momentum equations for incompressible flows are given in tensor notation and Cartesian coordinates by Eq (5) and Eq (6) (Ferziger and Peric, 2002).

$$\frac{\partial\left(\rho\overline{u}_i\right)}{\partial x_i} = 0, \tag{5}$$

$$\frac{\partial\left(\rho\overline{u}_i\right)}{\partial t} + \frac{\partial}{\partial x_j}\left(\rho\overline{u}_i\overline{u}_j + \rho\overline{u_i'u_j'}\right) = -\frac{\partial\overline{p}}{\partial x_i} + \frac{\partial\overline{\tau}_{ij}}{\partial x_j} \tag{6}$$

where ρ is density, $\overline{u}_i$ is the averaged Cartesian components of the velocity vector, $\rho\overline{u_i'u_j'}$ is the Reynolds stresses and p is the mean pressure. $\overline{\tau}_{ij}$ are the mean viscous stress tensor components, as shown in Eq (7).

$$\overline{\tau}_{ij} = \mu\left(\frac{\partial\overline{u}_i}{\partial x_j} + \frac{\partial\overline{u}_j}{\partial x_i}\right) \tag{7}$$

in which μ is the dynamic viscosity.

The solver uses a finite volume method which discretises the governing equations. A second order convection scheme was used for the momentum equations and a first order temporal discretisation was used. The flow equations were solved in a segregated manner. The continuity and momentum equations were linked with a predictor-corrector approach.

The SST (Shear Stress Transport) k-ω turbulence model was used in order to complete the RANS equations, which blends the k-ω model near the wall and the k-ε model in the far field. It is of note that the ITTC (2014) recommend the use of at least 180 time steps per revolution. Therefore, the time step size of the unsteady simulations was set such that the recommendation of ITTC (2014) was satisfied to ensure a reliable solution for such a complex phenomenon.
The wall-function approach proposed by Demirel et al. (2017a) was used throughout all the cases, by employing the roughness function model given by equation (8), for a range of representative coating and fouling conditions shown in Table 1.

$$\Delta U^{+} = \begin{cases} 0 & \rightarrow \quad k^{+} < 3 \\ \frac{1}{\kappa}\ln\left(0.26k^{+}\right)^{\sin\left[\frac{\pi}{2}\frac{\log(k^{+}/3)}{\log(5)}\right]} & \rightarrow \quad 3 < k^{+} < 15 \\ \frac{1}{\kappa}\ln\left(0.26k^{+}\right) & \rightarrow \quad 15 < k^{+} \end{cases} \tag{8}$$

Reference may be made to Demirel et al. (2017a) for a comprehensive explanation on the wall-function approach for fouling conditions used in this study. General information about the wall-function approach and details of the application of roughness functions through wall-functions can be found in Demirel et al. (2014).

Table 1 A range of representative coating and fouling conditions (Schultz, 2007).

Description of condition	NSTM rating*	k_s (μm)	Rt_{50} (μm)
Hydraulically smooth surface	0	0	0
Typical as applied AF coating	0	30	150
Deteriorated coating or light slime	10-20	100	300
Heavy slime	30	300	600
Small calcareous fouling or weed	40-60	1000	1000
Medium calcareous fouling	70-80	3000	3000
Heavy calcareous fouling	90-100	10000	10000

*NSTM (2002)

3.2. Geometry and boundary conditions

To aid in the advancement of numerical simulations in CFD packages, SVA Potsdam Model Basin in Germany published open water results for a model propeller they designed in 1998

called the VP1304 (SVA, 2011). It has become a standard propeller test case called Potsdam Propeller Test Case (PPTC), shown in Figure 2, where users can verify a numerical simulation against the published model experiment results. This propeller has been used extensively for research purposes in industry, with one such example being to analyse energy saving devices such as PBCF, short for Propeller Boss Cap Fins. Studies have outlined design and optimisation procedures using the PPTC results and CFD software to show possible energy efficiency increases of 1.3% (Mizzi et al., 2017). As there is a significant body of information available in the public domain for the PPTC propeller geometry and its open water tests, both the propeller and its shaft could be accurately represented in the validation study. Some main geometrical parameters of the PPTC propeller can be seen in Table 2.

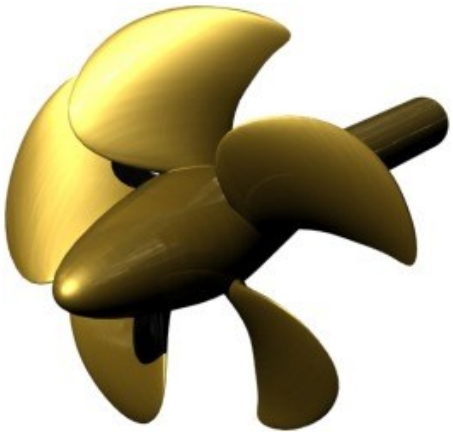

Figure 2 PPTC propeller (Mizzi et al., 2017).

Table 2 PPTC propeller parameters (adopted from SVA Postdam Model Basin, 2011).

Parameter	Symbol	Value
Diameter	D	0.250
Pitch Ratio r/R=0.7	$P_{0.7}/D$	1.635
Area Ratio	A_E/A_O	0.779
Chord Length$_{0.7}$ (m)	$C_{0.7}$	0.104
Skew (deg)	θ	18.837
Hub Ratio	D_h/D	0.300
No. of Blade	Z	5
Rotation	Direction	Right
Revolutions/s (rps)	n	15

It is important to choose appropriate boundary conditions for CFD problems, since these boundary conditions directly affect the accurate flow solutions (Demirel et al., 2014). A general view of the computation domain with the PPTC Model-Scale Propeller model and the notations of selected boundary conditions are depicted in Figure 3.

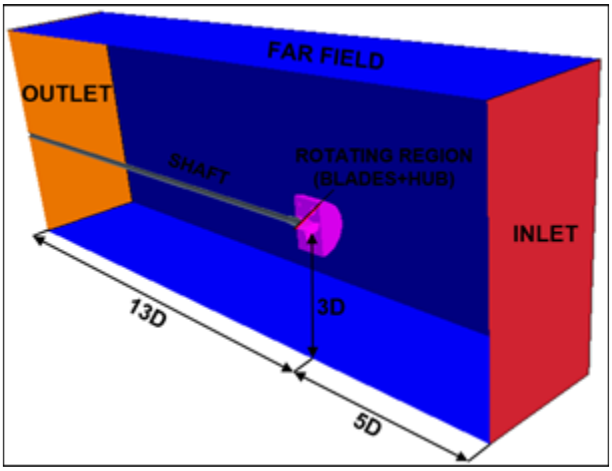

Figure 3 An overview of the domain with the selected boundary conditions.

The boundary conditions of the simulations were chosen to represent the propeller being completely submerged in an infinite ocean. Table 3 shows the regions and boundaries that the simulation is divided into and the type of boundary employed. This controls how the flow enters and exits the domain through the inlet and outlet and that the flow will slow due to boundary layer effects at a wall boundary. Whilst the far field symmetry condition tells the software the domain is infinite, i.e. not to consider the effect of the water surface or the seabed. Equally for the far field region a slip wall condition or a velocity inlet with its only component parallel to the flow direction would give the same results.

Table 3 Boundary conditions.

Regions	Boundaries	Type
Rotating	Blades	No-slip wall
	Hub	No-slip wall
Stationary	Far Field	Symmetry plane
	Inlet	Velocity inlet
	Outlet	Pressure outlet
	Shaft	No-slip wall

The propeller was modelled as a no-slip rough wall in order to represent the roughness on the propeller. The two opposite faces at the x-direction of the domain were modelled as a velocity inlet and a pressure outlet, respectively. Only half of the propeller and control volume were considered in CFD calculations by using a symmetry plane. This halves the required cell numbers and does not affect the computations.

Another critical selection is the positioning of the boundaries, especially the downstream outlet boundary and the upstream inlet boundary. The inlet is placed at ~5D length upstream and the outlet is placed at ~13D length downstream to avoid any reflections downstream of the propeller and to ensure uniform incoming flow upstream of the propeller, and according to CD-

Adapco (2014). The locations of the boundaries are shown in Figure 3, where D represents the propeller diameter. A distance of 5D allows the flow to be fully developed upon reaching the propeller whilst the larger distance of 13D behind the propeller captures the turbulent effect the rotational motion has on the water. Since the flow occurs in line with the shaft, this is the direction of interest so 3D above and below propeller is adequate. This figure also shows that the flow is uninterrupted upon entering the propeller which is the aim of an open water simulation. In the experimental setup, the recording devices and mountings would be seen on this shaft located behind the propeller.

3.3. Mesh generation

To yield reliable results from CFD calculations, the generation of an accurate mesh is of great importance. A cut-cell grid with prism layer mesh on the walls was generated using the automatic mesh generator in STAR-CCM+. Local refinement is carried out for the propeller blades region to capture finer details on this surface, with a finer mesh again at the blade edges as these surfaces produce more torque, thus are of more importance to achieve an accurate solution.

A coarse mesh was employed in the far field, inlet and outlet regions since the flow far from propeller is not as crucial on the results whereas an extra cylinder is created in the rotating region to capture rotational flow characteristics of the propeller. Figure 4 shows the profile cross-section of the meshed domain whereas Figure 5 shows the surface mesh. The mesh generation for this study was achieved using similar techniques to those explained in Demirel et al. (2014) and in Mizzi et al. (2017).

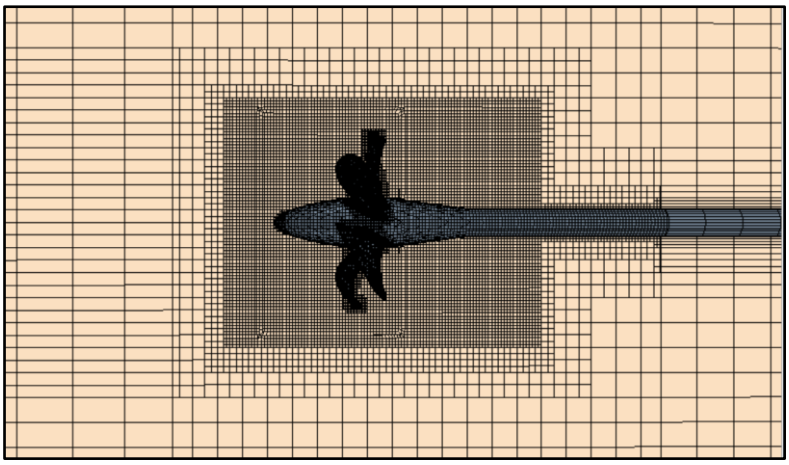

Figure 4 Profile view cross-section.

Figure 5: Surface mesh.

Performing near-wall mesh generation requires great care since this is directly related to the hull roughness due to marine coatings and biofouling. A special near-wall mesh resolution was applied to all surfaces with no-slip boundary conditions based on the roughness height values corresponding to each fouling condition. For this reason, the near-wall cell numbers varied for some of the fouling conditions. These differences resulted in different total cell numbers. According to CD-Adapco (2014) and Demirel et al. (2014, 2017a), the prism layer thickness and prism layer numbers were determined such that y^+ is always higher than 30, and higher than k^+. The numbers of the total cells generated are given in Table 4 for propeller.

Table 4 Total cell numbers.

Surface Condition (k_s [μm])	Cell numbers
k_s=0, k_s=30, k_s=100	$2.8x10^6$
k_s=300	$2.7x10^6$
k_s=1000 k_s=3000, k_s=10000	$2.0x10^6$

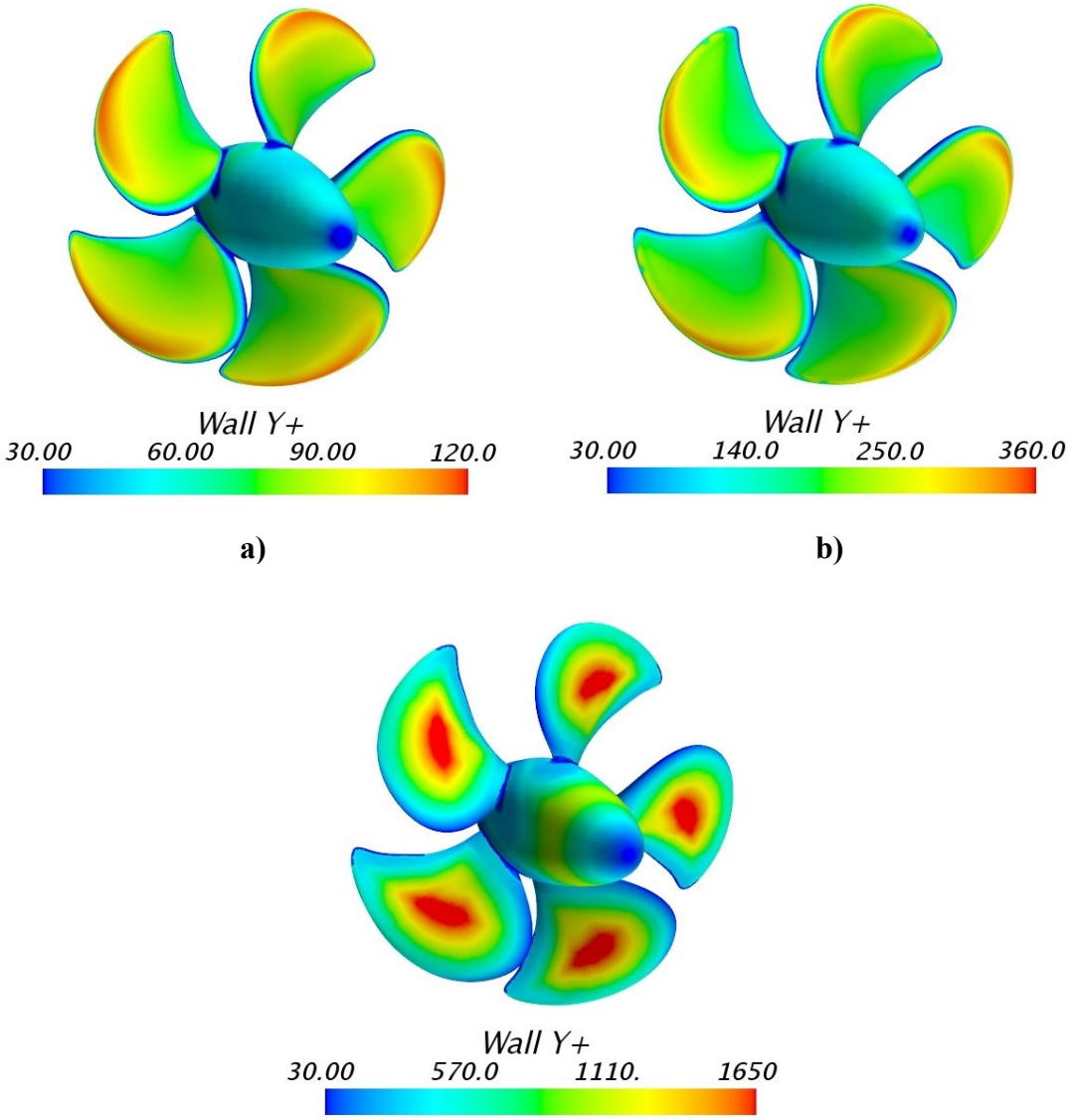

Figure 6 y^+ values on a) k_s=0, k_s=30, k_s=100, b) k_s=300, c) k_s=1000, ks=3000, k_s=10000 surfaces.

The final y^+ distribution on different surfaces is illustrated in Figure 6. It should be noted that although the y^+ ranges on the surfaces are extensive, the weighted average y^+ values are well below 100.

In addition to this, convergence tests were carried out in order to obtain grid independent solution. Since the cell numbers are influential on the solution, performing convergence tests is also necessary to be able to predict the uncertainty of the CFD calculations. The details and a discussion of the convergence test and near wall mesh dependence study are presented in Section 4.1.

3.4. Modelling Variations

CFD includes two possible methods to simulate a rotating propeller: the Moving Reference Frame (MRF) Method and the Rotating Mesh also known as Sliding Mesh approach. For the sliding mesh approach, the whole domain rotates about an axis yielding transient calculations producing time-accurate results that require high computational power. For the MRF approach which is less computationally expensive, the domain remains stationary with an assigned frame of reference rotating about a pre-defined axis with respect to the global co-ordinate system. MRF simulations carry out a steady-state approximation to a transient problem producing time-averaged results (Mizzi et al., 2017). In this study, a comparison study was carried out investigating the differences between the propeller representation methods, namely steady MRF, unsteady MRF and unsteady sliding mesh methods.

Table 7 presents the K_T, K_Q and η for each simulation in comparison with the experimental results given in Table 6. It should be noted that the experimental values given in Table 6 are experimental results interpolated for J values of interest, based on the original experimental data of SVA (2011) (see Table 5). It is of note that the term experimental data stands for the interpolated values given in Table 6 from this point onward.

Table 5 SVA (2011) experimental results.

J	K_T	$10K_Q$	η
0.5341	0.6667	1.4648	0.387
0.6676	0.5903	1.3251	0.473
0.7985	0.5117	1.1836	0.549
0.9314	0.4380	1.0493	0.619
1.0683	0.3641	0.9096	0.681
1.2021	0.2922	0.7676	0.728

Table 6 SVA (2011) experimental results interpolated for J values of interest.

J	K_T	$10K_Q$	η
0.6	0.6290	1.3958	0.4295
0.8	0.5109	1.1821	0.5498
1.0	0.4010	0.9793	0.6501
1.2	0.2933	0.7698	0.7273

Table 7 The comparison of modelling variations.

Steady MRF						
J	K_T	(%)Experiment K_T	$10K_Q$	(%)Experiment$10K_Q$	η	(%) Experiment η
0.6	0.6315	0.3982	1.4311	2.5292	0.4212	-1.92
0.8	0.5034	-1.4668	1.1962	1.1960	0.5356	-2.59
1.0	0.3797	-5.3153	0.9703	-0.9199	0.6225	-4.24
1.2	0.2630	-10.3374	0.7488	-2.7339	0.6706	-7.80
Unsteady MRF						
J	K_T	(%)Experiment K_T	$10K_Q$	(%)Experiment$10K_Q$	η	(%) Experiment η
0.6	0.6367	1.2229	1.4298	2.4361	0.4250	-1.03
0.8	0.5050	-1.1536	1.1983	1.3691	0.5364	-2.44
1.0	0.3802	-5.1691	0.9713	-0.8134	0.6228	-4.20
1.2	0.2637	-10.1148	0.7500	-2.5695	0.6711	-7.72
Unsteady Sliding Mesh						
J	K_T	(%)Experiment $10K_Q$	$10K_Q$	(%)Experiment$10K_Q$	η	(%) Experiment η
0.6	0.6331	0.6549	1.4218	1.8614	0.4250	-1.03
0.8	0.5024	-1.6591	1.1925	0.8784	0.5362	-2.47
1.0	0.3792	-5.4361	0.9688	-1.0702	0.6226	-4.22
1.2	0.2633	-10.2373	0.7493	-2.6645	0.6708	-7.76

Table 7 demonstrates the comparison between experimental and CFD results for the PPTC propeller characteristics. It is evident that using unsteady time model slightly increases the accuracy of the results compared to those obtained using steady time model. Having said that the use of unsteady model cause substantial run-time while slightly improving the accuracy. Another interesting observation is that the results obtained using sliding mesh and MRF methods showed minor differences, which is in accordance with the findings of Mizzi et al. (2017). Thus, the less computationally intensive steady and MRF model is retained. All of the open water efficiency results show good agreement for advance coefficients (J) between 0.6 to 1 with 4% accuracy; with the accuracy decreasing significantly outside this range. Due to CFD transition model simplifications, efficiency values are smaller than those obtained from the experiments outside this range. The RANS simulation model was set to assume a fully turbulent flow which failed to predict the transition behaviour in the boundary layer.

In order to have improved predictions of open water efficiency values, either a transition model could be employed into the simulation or tests could be carried out in full scale. Since the transition region within the boundary layer of a full scale model is less significant compared to model scale, modelling in full scale increases the accuracy. Having said that in this study only model scale simulations were carried out to eliminate the large numbers of cells which would cause significant additional run-time.

4. RESULTS

4.1. Grid sensitivity study

Firstly, a near-wall grid dependence study was carried out to determine the effect of y^+ on the calculated open water characteristics. To generate each mesh, the distance of the first grid from the rough wall was gradually changed, whilst keeping all other parameters the same. Open water characteristics from different simulations, each with a different y^+ value, are shown in Table 8. The y^+ values listed represent the weighted average of the y^+ distribution histograms.

Table 8 Open water characteristics at different y^+ values.

y^+=30						
J	K_T	(%) Experiment K_T	$10K_Q$	(%) Experiment $10K_Q$	η	(%) Experiment η
0.6	0.6315	0.3961	1.4311	2.5321	0.4212	-1.9342
0.8	0.5034	-1.4729	1.1962	1.1946	0.5356	-2.5884
1.0	0.3797	-5.3226	0.9703	-0.9202	0.6225	-4.2464
1.2	0.2630	-10.3287	0.7488	-2.7303	0.6706	-7.8017
y^+=35						
J	K_T	(%) Experiment K_T	$10K_Q$	(%) Experiment $10K_Q$	η	(%) Experiment η
0.6	0.6343	0.8398	1.4410	3.2382	0.4202	-2.1744
0.8	0.5062	-0.9260	1.2052	1.9521	0.5345	-2.7755
1.0	0.3826	-4.5999	0.9790	-0.0341	0.6217	-4.3707
1.2	0.2659	-9.3389	0.7574	-1.6161	0.6703	-7.8397
y^+=40						
J	K_T	(%) Experiment K_T	$10K_Q$	(%) Experiment $10K_Q$	η	(%) Experiment η
0.6	0.6360	1.1162	1.4484	3.7651	0.4192	-2.4044
0.8	0.5082	-0.5278	1.2120	2.5287	0.5337	-2.9337
1.0	0.3849	-4.0086	0.9864	0.7210	0.6208	-4.4994
1.2	0.2685	-8.4403	0.7652	-0.5915	0.6699	-7.8855
y^+=90						
J	K_T	(%) Experiment K_T	$10K_Q$	(%) Experiment $10K_Q$	η	(%) Experiment η
0.6	0.6245	-0.7148	1.4309	2.5162	0.4166	-3.0041
0.8	0.5089	-0.3822	1.2160	2.8672	0.5327	-3.1115
1.0	0.3952	-1.4449	1.0066	2.7861	0.6246	-3.9188
1.2	0.2845	-2.9882	0.7970	3.5322	0.6816	-6.2877

As demonstrated in Table 8, although the solutions slightly differ with varying y^+ values, the use of higher y^+ values to comply with the requirements related to severe fouling conditions does not cause significant deviations.

Systematic studies were then performed in order to carry out a grid sensitivity study and to predict the numerical uncertainties. In order to observe the effect of cell numbers on the key variables, (K_T, $10K_Q$ and η), the domain was discretised in four different resolutions and the simulations were run for each configuration. Four different types of mesh grid refinements were classified as coarser, coarse, medium, and fine. A mesh refinement factor, *r*, was chosen as $\sqrt{2}$ as used by Tezdogan et al., (2015),Peder Kavli et al. (2017) and Momchil et al. (2018).

K_T, $10K_Q$ and η values for each mesh configuration were computed and are presented in Table 9 and Figure 7.

Table 9 Open water characteristics at different mesh configurations.

	Coarser			*Coarse*			*Medium*			*Fine*		
Cell Number	*1.3 M*			*1.8 M*			*2.7 M*			*4.3 M*		
J=0.6	K_T	$10K_Q$	η	K_T	$10K_Q$	η	K_T	$10K_Q$	η	K_T	$10K_Q$	η
Results	0.6257	1.4252	0.4190	0.6286	1.4280	0.4202	0.6315	1.4311	0.4212	0.6343	1.4347	0.4220
(%) Experiment	*-0.52*	*2.11*	*-2.44*	*-0.06*	*2.31*	-2.17	0.40	2.53	-1.93	*0.84*	*2.79*	*-1.75*

**(%) Experiment* represents the difference between the numerical results and the experimental values.

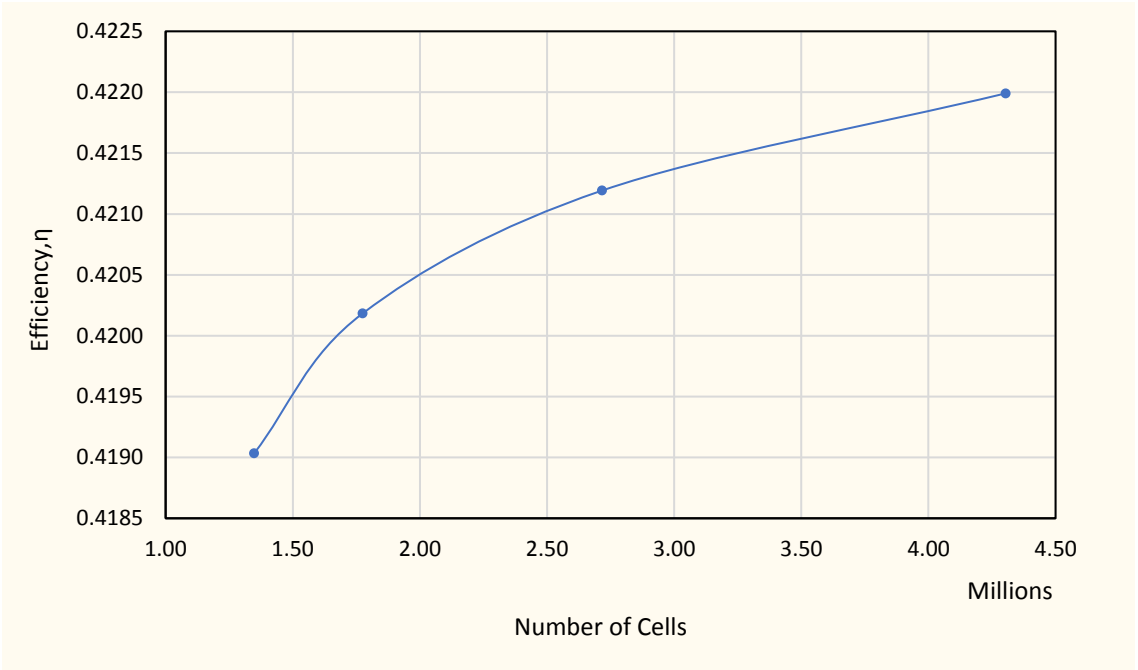

Figure 7 Grid dependence.

Table 9 and Figure 7 show that increasing the cell count brings the solution closer to that of the experimental result but with detrimental penalties in run time. Medium mesh configuration was found to be the best compromise between the accuracy and run-time and therefore medium mesh configuration was selected in all subsequent computations. (The error for open water efficiency versus experimental result at J=0.6 is 1.93 %).

Table 9 highlights that the mesh dependence study showed monotonic convergence, this is deemed to occur when further refinements bring the result closer and closer to a final solution, i.e. there are no signs of oscillations or divergence.

4.2. Verification study

A verification study should be carried out to show the capability of the proposed model and the software for the desired calculations. The Grid Convergence Index (GCI) Method based on

Richardson extrapolation (Richardson (1910), Richardson and Gaunt (1927)) was used in this paper's work for discretisation error estimation as described by Celik et al. (2008).

The apparent order of the method, p_a, is calculated by

$$p_a = \frac{1}{\ln(r_{21})}\left|\ln\left|\varepsilon_{32}/\varepsilon_{21}\right| + q(p_a)\right| \tag{9}$$

$$q(p_a) = \ln\left(\frac{r_{21}^{p_a} - s}{r_{32}^{p_a} - s}\right) \tag{10}$$

$$s = 1 \cdot sign\left(\varepsilon_{32}/\varepsilon_{21}\right) \tag{11}$$

where r_{21} and r_{32} are refinement factors, i.e. $\sqrt{2}$ in this study, and $\varepsilon_{32}=\phi_3-\phi_2$, $\varepsilon_{21}=\phi_2-\phi_1$, ϕ_k is the key variable, i.e. K_T and K_Q in this case, on the k^{th} grid.
The extrapolated values are obtained by

$$\phi_{ext}^{21} = \left(r_{21}^p\phi_1 - \phi_2\right)/\left(r_{21}^p - 1\right) \tag{12}$$

The approximate and extrapolated relative errors are calculated using the following equations, respectively.

$$e_a^{21} = \left|\frac{\phi_1 - \phi_2}{\phi_1}\right| \tag{13}$$

$$e_{ext}^{21} = \left|\frac{\phi_{ext}^{12} - \phi_1}{\phi_{ext}^{12}}\right| \tag{14}$$

The fine-grid convergence index is calculated by

$$GCI_{fine}^{21} = \frac{1.25e_a^{21}}{r_{21}^p - 1} \tag{15}$$

The required parameters were calculated for K_T and K_Q values and are presented in Table 10.

Table 10 Calculation of the discretion error for K_T and K_Q values.

	K_T	K_Q
r_{21}, r_{32}	√2	√2
ϕ_1	0.14311	0.63150
ϕ_2	0.14280	0.62900
ϕ_3	0.14252	0.62600
p_a	0.29368	0.52607
ϕ_{ext}^{21}	0.14600	0.64400
e_a^{21}	0.2166%	0.3959%
e_{ext}^{21}	1.9817%	1.9410%
GCI_{fine}^{21}	2.5272%	2.4743%

As can be seen from Table 10, numerical uncertainties of 2.52%, 2.47% were calculated for the computed K_T and K_Q values respectively.

4.3 Validation study

This section presents the results of the CFD simulation showing the open water propeller characteristics of PTTC propeller compared to the experimental results (SVA, 2011). Figure 8 presents these results in a graph, where the experimental values are shown by the black lines and CFD values by the red lines.

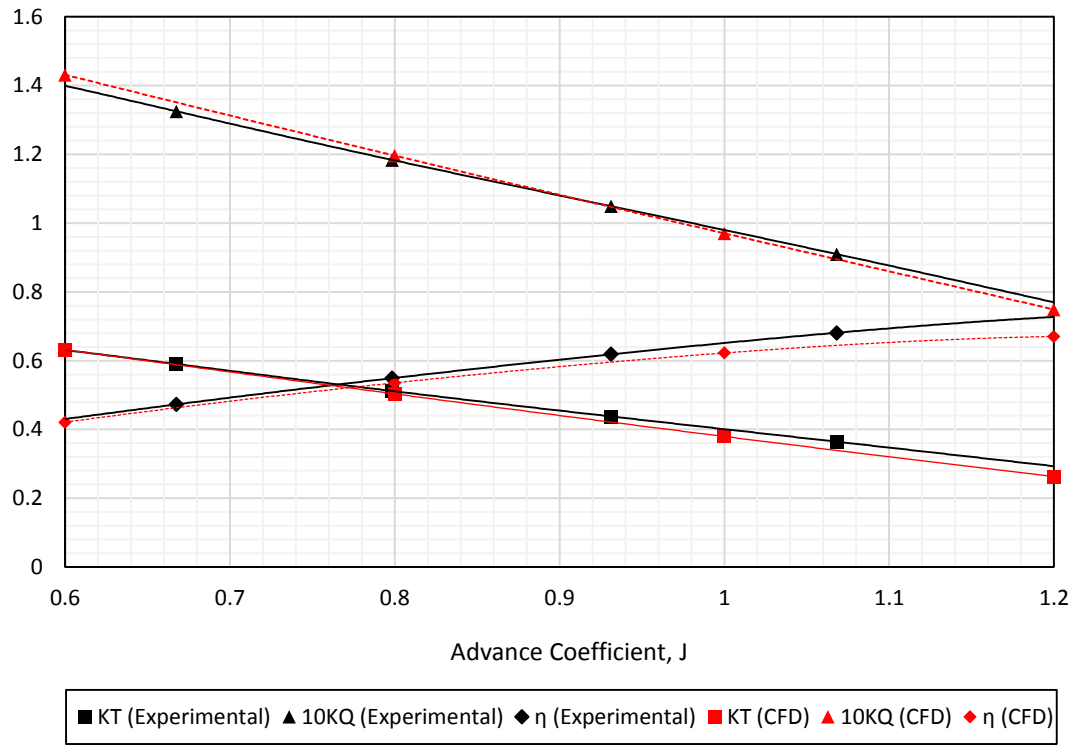

Figure 8 PPTC open water characteristics.

From Figure 8, it is clear there is a good agreement between experimental and CFD results. There is a slight over estimation of K_T and $10K_Q$ at low J values and conversely a slight underestimation at high J values. The efficiency exhibits the largest deviation at high J values since it incorporates both K_T and $10K_Q$ and possible inaccuracies with these results. Another conclusion is that at higher y^+ values, the accuracy of the simulation slightly reduces. Since y^+ is a function of shear stress and velocity, the increased velocity of higher J values could be the reason for this slight disagreement.

4.4 Effects of fouling

In this section the effects of different roughness conditions of the propeller are presented. Thrust coefficient (K_T), torque coefficient (K_Q) and propulsion efficiency (η) values of the model scale PPTC propeller were directly predicted by the present CFD simulations. Open water characteristics in the case of smooth condition are outlined in Table 11.

Table 11 Open water characteristics for smooth condition.

Hydraulically smooth surface			
J	K_T	$10K_Q$	η
0.6	0.6315	1.4311	0.4212
0.8	0.5034	1.1962	0.5356
1.0	0.3797	0.9703	0.6225
1.2	0.2630	0.7488	0.6706

Table 12 demonstrates the change in the open water characteristics of the PPTC propeller due to different surface conditions with respect to smooth condition. As can be seen from Table 12, thrust coefficient (K_T) continuously decreased with increasing fouling rates while torque coefficient (K_Q) continuously increased with increasing fouling rates.

Table 12 Comparison of the computed open water characteristics.

Typical as applied AF coating						
J	K_T	(%) Smooth K_T	$10K_Q$	(%) Smooth $10K_Q$	η	(%) Smooth η
0.6	0.6242	-1.16	1.4348	0.26	0.4153	-1.40
0.8	0.4951	-1.65	1.1981	0.16	0.5259	-1.80
1.0	0.3699	-2.58	0.9702	-0.01	0.6065	-2.58
1.2	0.2511	-4.52	0.7457	-0.41	0.6429	-4.12
Deteriorated coating or light slime						
J	K_T	(%) Smooth K_T	$10K_Q$	(%) Smooth$10K_Q$	η	(%) Smooth η
0.6	0.6115	-3.17	1.4417	0.74	0.4049	-3.88
0.8	0.4820	-4.25	1.2041	0.66	0.5095	-4.87
1.0	0.3566	-6.08	0.9769	0.68	0.5807	-6.72
1.2	0.2367	-10.00	0.7515	0.36	0.6014	-10.31
Heavy Slime						
J	K_T	(%) Smooth K_T	$10K_Q$	(%) Smooth $10K_Q$	η	(%) Smooth η
0.6	0.5926	-6.15	1.4345	0.24	0.3943	-6.38
0.8	0.4633	-7.97	1.2006	0.37	0.4911	-8.31
1.0	0.3351	-11.74	0.9694	-0.09	0.5499	-11.66
1.2	0.2120	-19.37	0.7382	-1.41	0.5484	-18.22
Small calcareous fouling or weed						
J	K_T	(%) Smooth K_T	$10K_Q$	(%) Smooth $10K_Q$	η	(%) Smooth η
0.6	0.5665	-10.30	1.4443	0.92	0.3744	-11.11
0.8	0.4424	-12.11	1.2254	2.43	0.4596	-14.19
1.0	0.3195	-15.85	1.0096	4.05	0.5034	-19.14
1.2	0.2017	-23.32	0.7978	6.54	0.4826	-28.03
Medium calcareous fouling						
J	K_T	(%) Smooth K_T	$10K_Q$	(%) Smooth $10K_Q$	η	(%) Smooth η
0.6	0.5627	-10.89	1.4483	1.20	0.3709	-11.94
0.8	0.4377	-13.05	1.2278	2.64	0.4538	-15.28
1.0	0.3141	-17.27	1.0117	4.26	0.4938	-20.67
1.2	0.1959	-25.50	0.8005	6.90	0.4672	-30.33
Heavy calcareous fouling						
J	K_T	(%) Smooth K_T	$10K_Q$	(%) Smooth $10K_Q$	η	(%) Smooth η
0.6	0.5627	-10.89	1.4483	1.20	0.3709	-11.94
0.8	0.4377	-13.05	1.2278	2.64	0.4538	-15.28
1.0	0.3141	-17.27	1.0117	4.26	0.4938	-20.67
1.2	0.1959	-25.50	0.8005	6.90	0.4672	-30.33

As can be seen in Table 12, the decreases in the efficiency of the propeller were predicted to be 1.40% at J=0.6 and 4.12% at J=1.2 for a typical as applied antifouling (AF) coating, 3.88% at J=0.6 and 10.31% at J=1.2 for a light slime condition and 11.94% at J=0.6 and 30. 33% at J=1.2 for a heavy calcareous fouling condition. These values altered to 6.38%, 11.11% and 11.94% at J=0.6 and 18.22%, 28.03% and 30.33% at J=1.2 for heavy slime, small calcareous fouling or weed and medium calcareous fouling, respectively.

The results presented in Table 12 indicate that the reduction in the K_T of the propeller due to a typical, as applied AF coating were predicted to be 1.16% and 4.52% whereas those due to a deteriorated coating or light slime were computed to be 3.17% and 10% at J values of 0.6 and 1.2, respectively. It was shown that the effect of heavy slime on the PPTC propeller caused a reduction in the K_T of 6.15% at J=0.6 and 19.37% at J=1.2. The calcareous fouling would decrease K_T by up to 10.89% at J=0.6 and 25.50% at J=1.2.

Similarly, the increase in the torque coefficient, K_Q, of the PPTC propeller due to a deteriorated coating or light slime surface condition was predicted to be 0.74% at a J value of 0.6 and to be 0.36% at a J value of 1.2. These values became 0.24% and 1.41% when calculating the increase in K_Q due to a heavy slime condition. Calcareous fouling causes significant increase in K_Q values, ranging from 0.92% to 1.20% at J=0.6 and 6.54% to 6.90% at J=1.2, depending on the type of calcareous fouling and ship speed.

An interesting point to note is that the effects of medium calcareous fouling and heavy calcareous fouling on the open water characteristics of the model-scale PPTC propeller are surprisingly similar. This can be attributed to the fact that the roughness heights of these fouling conditions are substantially high compared to the dimensions of the model-scale propeller and that open water characteristics are expected to reach a plateau at a certain fouling condition. The authors believe the outcome suggests that after a certain threshold, a further increase in the severity of fouling has a minor effect on open water characteristics.

Figure 9, Figure 10 and Figure 11 show the computed open water characteristics of the propeller obtained for seven different roughness conditions. Figure 9 highlights the thrust the propeller produces reduces with increased fouling severity. Small calcareous fouling or weed, medium calcareous fouling and heavy calcareous fouling conditions also become increasingly close together as the effect tails off once small calcareous fouling or weed is reached.

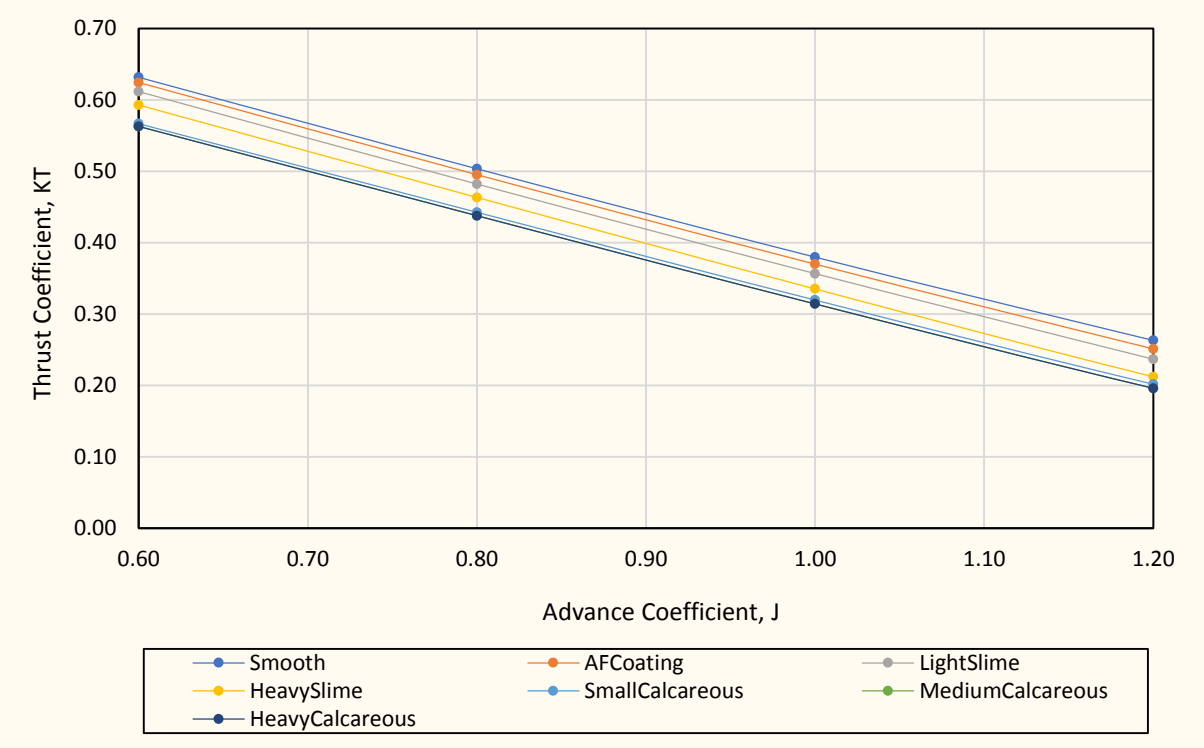

Figure 9 K_T values for different surface conditions.

Figure 10 shows the calculated torque coefficients, K_Q, of the PPTC propeller obtained for 7 different roughness conditions over an advance coefficient range from 0.6-1.2. As can be seen from Figure 10 and Table 12, the change in torque coefficients is lower than that observed for thrust coefficients. Results also showed that there is a tendency for the torque coefficient to increase with increasing surface roughness.

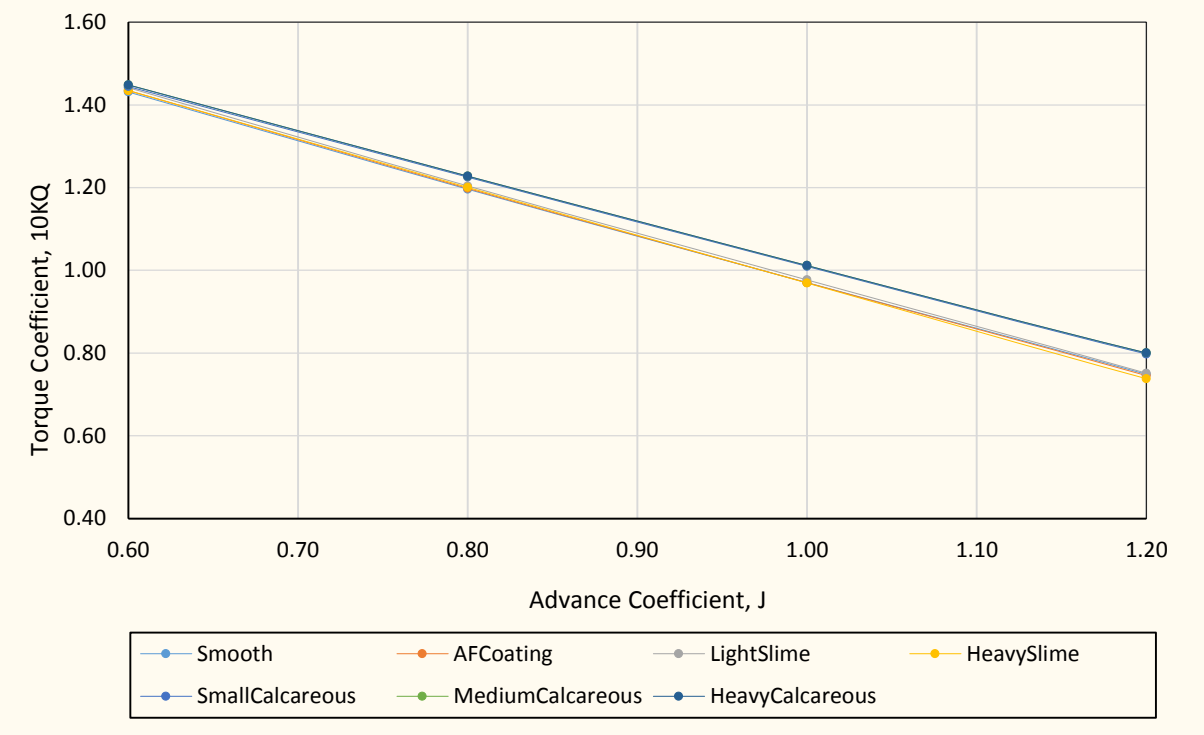

Figure 10 $10K_Q$ values for different surface conditions.

Figure 11 shows the decrease in efficiency through smooth condition to small calcareous fouling case and then that reduction diminishes from small calcareous fouling case to medium calcareous fouling case before finally medium calcareous fouling case and heavy calcareous fouling case lie on the same line so are plotted together. This graph indicates that the higher the J value the greater the reduction in efficiency, thus vessels operating at high advance coefficients will experience a greater effect on performance. The optimum efficiency point shifts towards lower J values with increased fouling and this can also be observed here.

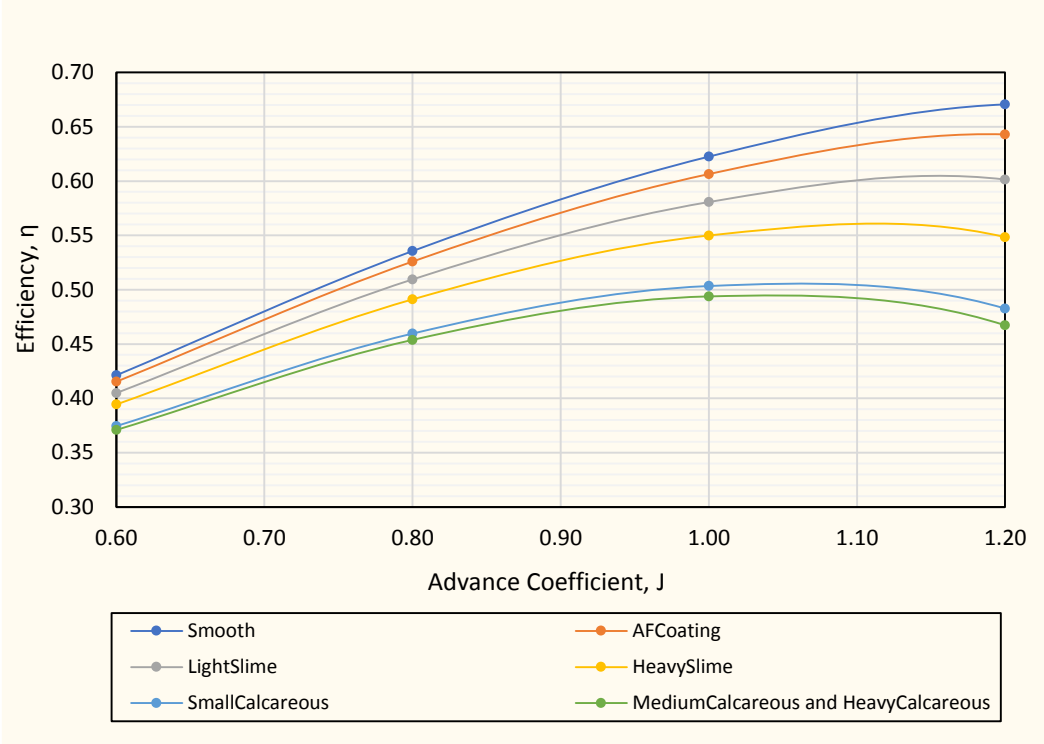

Figure 11 Efficiency comparison for different surface conditions.

Figure 12 also shows the increased efficiency drop at higher J values, with the J = 1.2 curve following a much sharper decline than the J = 0.6 curve as fouling severity increases. It is conclusive that between small calcareous fouling case and medium calcareous fouling case the efficiency loss plateaus for all J values and no longer increases with roughness.

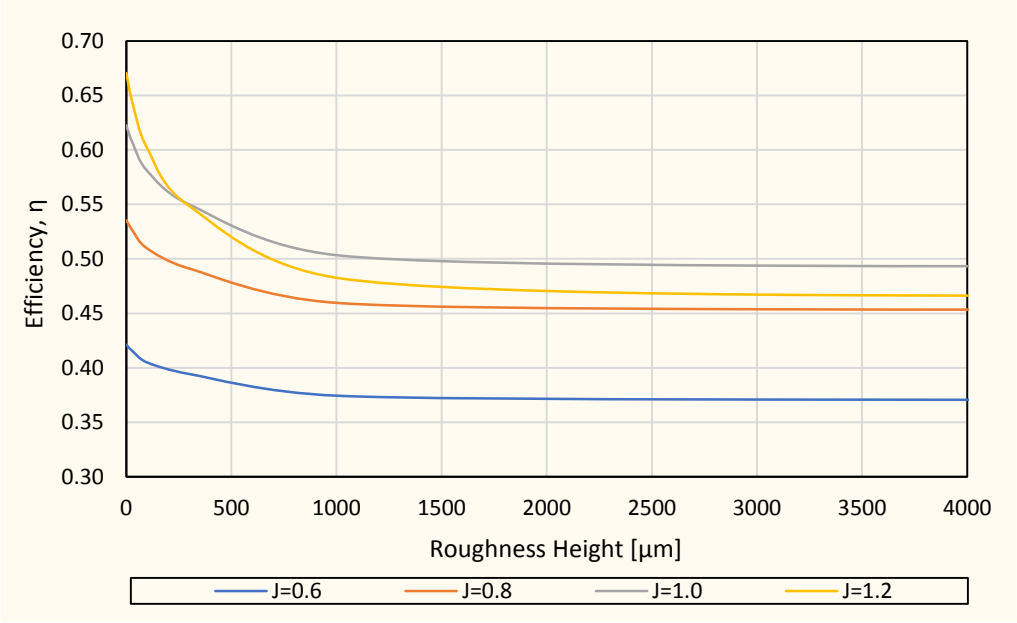

Figure 12 Efficiency for varying J values.

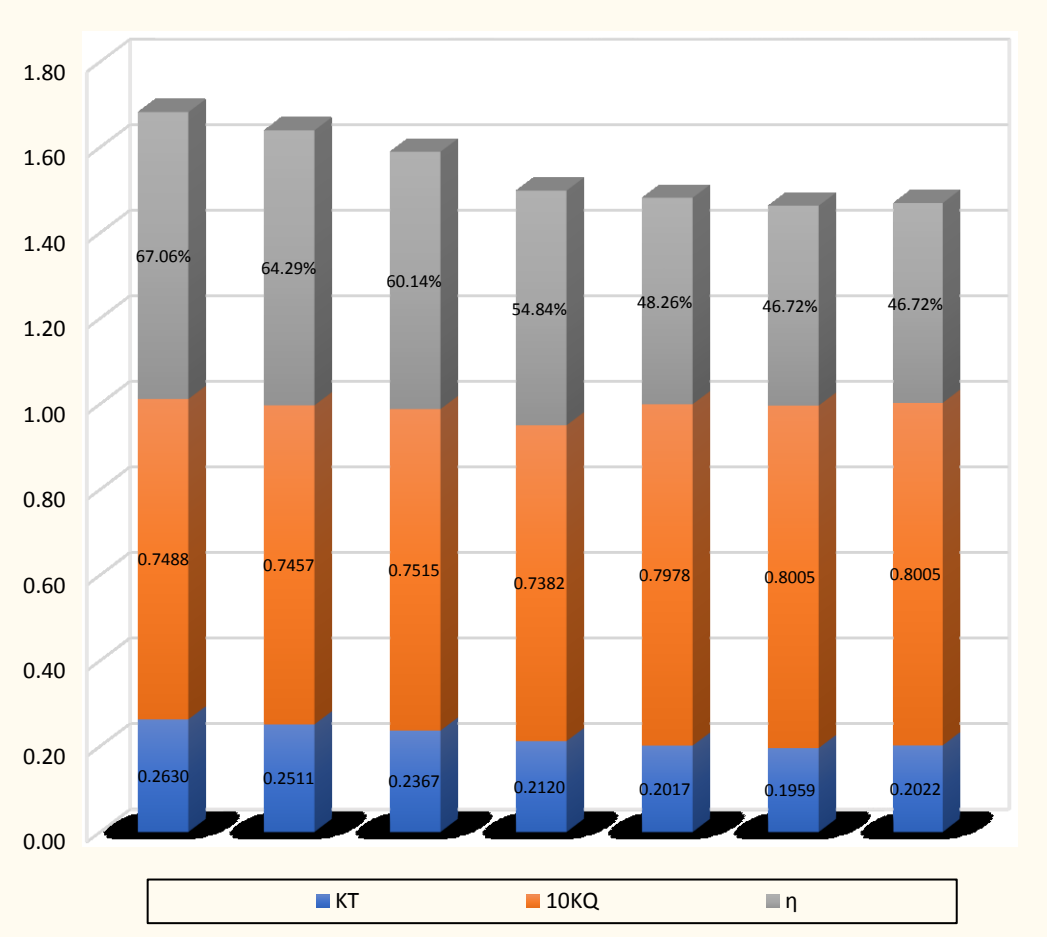

Figure 13 Open water characteristics for different surface conditions at J=1.2.

Figure 13 is useful in showcasing all three open water characteristics in one plot allowing the variation in each to be demonstrated. J = 1.2 was chosen as the clearest difference between fouling conditions occurs here.

5. DISCUSSION AND CONCLUSIONS

In this paper, a CFD approach for the prediction of propeller open water characteristics has been described using a well-known bench-marking case, namely the PPTC propeller. The propeller model was simulated with different levels of fouling applied in the form of a modified wall-function employing a new roughness function model. Model scale CFD optimisation was performed which provided valuable insights into the importance of various configurations, meshes and physics models. The paper reported very close agreement between the experimental results and CFD predictions for smooth condition.

Results showed that with increasing propeller surface fouling, the magnitude of the propeller thrust coefficient decreases while the magnitude of the torque coefficient increases. This results in a net decrease in open water efficiency of up to 30% at the highest simulated fouling level. The decreases in the efficiency of the propeller were predicted to be 1.40% at J=0.6 and 4.12% at J=1.2 for a typical as applied antifouling (AF) coating, 3.88% at J=0.6 and 10.31% at J=1.2 for a light slime condition and 11.94% at J=0.6 and 30.33% at J=1.2 for a heavy calcareous fouling condition. These values altered to 6.38%, 11.11% and 11.94% at J=0.6 and 18.22%, 28.03% and 30.33% at J=1.2 for heavy slime, small calcareous fouling or weed and medium calcareous fouling, respectively.

An interesting point to note is that the effects of medium calcareous fouling and heavy calcareous fouling on the open water characteristics of the model-scale PPTC propeller are surprisingly similar. This can be attributed to the fact that the roughness heights of these fouling conditions are substantially high compared to the dimensions of the model-scale propeller and that open water characteristics are expected to reach a plateau at a certain fouling condition. The authors believe the outcome suggests that after a certain threshold, increase in the severity of fouling have minor effect on open water characteristics.

It is important to highlight that the roughness function model used in this study was derived from the experimental data of flat plates where the boundary layer flow is developed along the main streamwise direction and the influence of pressure gradient is assumed to be negligible, while the flow conditions of propellers are different. Therefore, an obvious future work would be to carry out an experimental study including propellers covered with the biofouling conditions in question and to validate this CFD approach with the measured experimental data.

Having said that, the present CFD model and predictions may be considered as a leap forward towards a fully-nonlinear and realistic approach.

It should be noted that in this study, a uniform inflow was assumed into the propeller, which is not representative of a real case. In reality the propeller would not only be operating in the wake of a ship hull but also most likely a fouled ship hull, further changing the operational conditions away from the design point by modifying the wake, and hence further impacting on the propeller efficiency.

The approach proposed in this study can be extended in order to investigate other scenarios. Firstly, the use of roughness functions is not limited to propeller surfaces, but could be applied to hull and appendage surfaces. The impact of fouling on many other aspects of ship operation such as propeller efficiency behind a clean or fouled hull, ship manoeuvring, and seakeeping. Secondly, although the current approach applied a uniform coverage of one fouling level across the propeller, the method allows for non-uniform coverage and variation in fouling level over a surface. Thirdly, rather than using a single roughness height to represent a limited number of fouling types, a graduated approach could be developed to represent any level of fouling. In addition to the many applications of the approach, the addition of surface roughness has no impact on the running time of the CFD simulations and is therefore a cost effective and practical method for more realistic representation of reality. Using the approach described in this paper, ship owners could investigate the impact of fouling on their own propeller designs, and could hence use the efficiency changes predicted within a decision-making framework to schedule when it would be economically beneficial to dry dock the vessel or at least clean the propeller. An interesting future work will be to extend the CFD study to provide full scale predictions.

ACKNOWLEDGEMENTS

Results were obtained using the EPSRC funded ARCHIE-WeSt High Performance Computer (www.archie-west.ac.uk). EPSRC grant no. EP/K000586/1.

REFERENCES

Anderson, C., Atlar, M., Callow, M., Candries, M., Milne, A., Townsin, B., . 2003. The development of foul-release coatings for seagoing vessels. Proceedings of the Institute of Marine Engineering, Science and Technology Part B: Journal of Marine Deisgn and Operations January 2003 (No B4), 11-23.

Apsley, D., 2007. CFD Calculation of Turbulent Flow with Arbitrary Wall Roughness. Flow, Turbulence and Combustion 78 (2), 153-175.

Atlar, M., Anderson, C.D., Candries, M., Glover, G.J., Mutton, R.J., 2003a. The effect of a foul release coating on propeller performance, Environmental Sustainability (ENSUS), University of Newcastle upon Tyne, Newcastle upon Tyne.

Atlar, M., Anderson, C.D., Glover, E.J., Mutton, R.J., 2003b. Calculation of the Effects of New Generation Coatings on High Speed Propeller Performance, 2nd International Warship Cathodic Protection Symposium and Equipment Exhibition, Shrivenham, UK.

Aupoix, B., 2007. A general strategy to extend turbulence models to rough surfaces: application to Smith's k-L model. Journal of Fluids Engineering 129 (10), 1245-1254.

Castro, A.M., Carrica, P.M., Stern, F., 2011. Full scale self-propulsion computations using discretized propeller for the KRISO container ship KCS. Computers & Fluids 51 (1), 35-47.

CD-Adapco, 2014 StAR-CCM+, User Guide, version 9.0.2.

Cebeci, T., Bradshaw, P., 1977. Momentum Transfer in Boundary Layers. Hemisphere Publishing Corporation/McGraw-Hill.

Celik, I.B., Ghia, U., Roache, P.J., Freitas, C.J., Coleman, H., Raad, P.E., 2008. Procedure for estimation and reporting of uncertainty due to discretization in CFD applications. Journal of Fluids Engineering-Transactions of the ASME 130 (7), 078001-078001-078004.

Demirel, Y.K., 2015. Modelling the roughness effects of marine coatings and biofouling on ship frictional resistance, Department of Naval Architecture, Ocean and Marine Engineering. University of Strathclyde.

Demirel, Y.K., Khorasanchi, M., Turan, O., Incecik, A., Schultz, M.P., 2014. A CFD model for the frictional resistance prediction of antifouling coatings. Ocean Engineering 89, 21-31.

Demirel, Y.K., Turan, O., Day, S., 2015. Experimental determination of added hydrodynamic resistance caused by marine biofouling on ships, 4th International Conference on Advanced Model Measurement Technologies for the Maritime Industry, Istanbul, Turkey.

Demirel, Y.K., Turan, O., Incecik, A., 2017a. Predicting the effect of biofouling on ship resistance using CFD. Applied Ocean Research 62, 100-118.

Demirel, Y.K., Uzun, D., Zhang, Y., Fang, H.C., Day, A.H., Turan, O. 2017b. Effect of barnacle fouling on ship resistance and powering. Biofouling, 33:10, 819-834, DOI: 10.1080/08927014.2017.1373279.

Eça, L., Hoekstra, M., 2011. Numerical aspects of including wall roughness effects in the SST k–ω eddy-viscosity turbulence model. Computers & Fluids 40 (1), 299-314.

Fang, I., Cheng, F., Incecik, A., Carnie, P. 2013. Global Marine Trends 2030 1st Edition. QinetiQ / Lloyd's Register / University of Strathclyde, ed., London. Available at : http://www.futurenautics.com/wp- content/uploads/2013/10/GlobalMarineTrends2030Report.pdf.

Ferziger, J.H., Peric, M., 2002. Computational Methods for Fluid Dynamics. Springer.

Granville, P.S., 1958. The frictional resistance and turbulent boundary layer of rough surfaces. Journal of Ship Research 2, 52-74.

Granville, P.S., 1978. Similarity-law characterization methods for arbitrary hydrodynamic roughnesses. Final Report Naval Ship Research and Development Center, Bethesda, MD. Ship Performance Dept. 1.

Grigson, C., 1985. The drag at ship scale of planes having any quality of roughness. Journal of Ship Research 29 (2), 94-104.

Haase, M., Zurcher, K., Davidson, G., Binns, J.R., Thomas, G., Bose, N., 2016. Novel CFD-based full-scale resistance prediction for large medium-speed catamarans. Ocean Engineering 111, 198-208.

Hansen, H.R., Dinham-Peren, T., Nojiri, T., 2011. Model and Full Scale Evaluation of a 'Propeller Boss Cap Fins' Device Fitted to an Afromax Tanker, Symposium on Marine.

Hydrex, 2017. Propeller Cleaning. Hydrex Underwater Technology.

ICCT, 2011. Reducing Greenhouse Gas Emissions from Ships - Cost Effectiveness Available Options, White Paper Number 11.

IMO, 2009. Second IMO GHG Study 2009, London,UK.

IMO, 2014. Annex 5, Resolution MEPC.245(66), 2014 Guidelines on the method of calculation of the attained Energy Efficiency Design Index (EEDI) for new ships. Marine Environment Protection Committee, http://www.imo.org/KnowledgeCentre/IndexofIMOResolutions/MEPC%20Resolutions/MEPC%20245%2066.pdf.

ITTC, 1990. Report of the Powering Performance Committee, Proceedings of the 19th ITTC. http://ittc.info/media/2304/report-of-the-power-performance-committee.pdf.

ITTC, 2011a. Performance, Propulsion 1978 ITTC Performance Prediction Method, ITTC Recommended Procedures.

ITTC, 2011b. Practical Guidelines for Ship CFD Application, ITTC Recommended Procedures and Guidelines, Procedure 7.5-03-02-03, Revision 01.

ITTC, 2014. Recommended Procedures and Guidelines - Practical Guidelines for Ship CFD Applications, Section 7.5-03-02-03. International Towing Tank Conference.

Kawamura, T., Ouchi, K., Nojiri, T., 2012. Model and Full SCale CFD Analysis of Propeller Boss Cap Fins (PBCF), J Mar Sci Technol, Japan.

Khor, Y.S., Xiao, Q., 2011. CFD simulations of the effects of fouling and antifouling. Ocean Engineering 38 (10), 1065-1079.

Korkut, E., Atlar, M., 2012. An experimental investigation of the effect of foul release coating application on performance, noise and cavitation characteristics of marine propellers. Ocean Engineering 41, 1-12.

Krogstad, P.-A., 1991. Modification of the van Driest damping function to include the effects of surface roughness. AIAA Journal 29 (6), 888-894.

Mizzi, K., Demirel, Y.K., Banks, C., Turan, O., Kaklis, P., Atlar, M., 2017. Design optimisation of Propeller Boss Cap Fins for enhanced propeller performance. Applied Ocean Research 62, 210-222.

Momchil, T., Tezdogan, T., Oguz, E., Gourlay, T., Demirel, Y.K., Incecik, A., 2018. Numerical investigation of the behaviour and performance of ships advancing through restricted shallow waters. Journal of Fluids and Structures 76, 185-215.

Mosaad, M.A., 1986. Marine Propeller Roughness Penalties, Naval Architecture and Shipbuilding. University of Newcastle upon Tyne, https://theses.ncl.ac.uk/dspace/handle/10443/1006.

Naval Ships' Technical Manual, 2002. Waterborne underwater hull cleaning of navy ships. S9086-CQ-STM-010/CH-081R5. Naval Sea Systems Command.

Nikuradse, J., 1933. Laws of flow in rough pipes. NACA Technical Memorandum 1292.

Patel, V.C., 1998. Perspective: Flow at high reynolds number and over rough surfaces—Achilles heel of CFD. Journal of Fluids Engineering 120 (3), 434-444.

Patience, G., Atlar, M., 1998. An Investigation into Effective Boss Cap Designs to Eliminate Propeller Hub Vortex Cavitation.

Peder Kavli, H., Oguz, E., Tezdogan, T., 2017. A comparative study on the design of an environmentally friendly RoPax ferry using CFD. Ocean Engineering 137, 22-37.

Richardson, L.F., 1910. The approximate arithmetical solution by finite differences of physical problems involving differential equations, with an application to the stresses in a masonry dam. Transactions of the Royal Society of London. Series A 210, 307-357.

Richardson, L.F., Gaunt, J.A., 1927. The deferred approach to the limit. Philosophical Transactions of the Royal Society of London. Series A 226, 299-361.

Schuiling, B., 2013. The Design and Numerical Demonstration of a New Energy Saving Device, 16th Numerical Towing Tank Symposium.

Schultz, M.P., 2007. Effects of coating roughness and biofouling on ship resistance and powering. Biofouling 23 (5), 331-341.

Seo, K.-C., Atlar, M., Goo, B., 2016. A Study on the Hydrodynamic Effect of Biofouling on Marine Propeller. Journal of the Korean Society of Marine Environment & Safety 22 (1), 123-128.

Suga, K., Craft, T.J., Iacovides, H., 2006. An analytical wall-function for turbulent flows and heat transfer over rough walls. International Journal of Heat and Fluid Flow 27 (5), 852-866.

SVA, 2011. Potsdam Propeller Test Case (PPTC) - Open Water Tests with the Model Propeller VP1304. Schiffbau-Versuchsanstalt Potsdam (SVA) Potsdam Model Basin.

Tezdogan, T., Demirel, Y.K., Kellett, P., Khorasanchi, M., Incecik, A., Turan, O., 2015. Full-scale unsteady RANS CFD simulations of ship behaviour and performance in head seas due to slow steaming. Ocean Engineering 97 (0), 186-206.

Townsin, R.L., Byrne, D., Svensen, T.E., Milne, A., 1981. Estimating the Technical and Economic Penalties of Hull and Propeller Roughness. SNAME, SNAME Transactions, pp. 295-318.